Inorg. Chem. **2003**, *42*, 5645–5653

One- and Two-Step Spin-Crossover Behavior of $[Fe^{II}(isoxazole)_6]^{2+}$ and the Structure and Magnetic Properties of Triangular $[Fe^{III}_3O(OAc)_6(isoxazole)_3][ClO_4]$

Wendy Hibbs, Petra J. van Koningsbruggen,† Atta M. Arif, William W. Shum, and Joel S. Miller*

Department of Chemistry, University of Utah, 315 S. 1400 E. RM Dock, Salt Lake City, Utah 84112-0850

Received February 28, 2003

The structure and spin-crossover magnetic behavior of $[Fe^{II}\mathbf{1}_6][BF_4]_2$ (**1** = isoxazole) and $[Fe^{II}\mathbf{1}_6][ClO_4]_2$ have been studied. $[Fe^{II}\mathbf{1}_6][BF_4]_2$ undergoes two reversible spin-crossover transitions at 91 and 192 K, and is the first two-step spin transition to undergo a simultaneous crystallographic phase transition, but does not exhibit thermal hysteresis. The single-crystal structure determinations at 260 [space group $P\bar{3}$, $a = 17.4387(4)$ Å, $c = 7.6847(2)$ Å] and at 130 K [space group $P\bar{1}$, $a = 17.0901(2)$ Å, $b = 16.7481(2)$ Å, $c = 7.5413(1)$ Å, $\alpha = 90.5309(6)°$, $\beta = 91.5231(6)°$, $\gamma = 117.8195(8)°$] reveal two different iron sites, Fe1 and Fe2, in a 1:2 ratio. The room-temperature magnetic moment of 5.0 μ_B is consistent with high-spin Fe(II). A plateau in $\mu(T)$ having a moment of 3.3 μ_B centered at 130 K suggests a mixed spin system of some high-spin and some low-spin Fe(II) molecules. On the basis of the Fe–N bond distances at the two temperatures, and the molar fraction of high-spin molecules at the transition plateau, Fe1 and Fe2 can be assigned to the 91 and 192 K transitions, respectively. $[Fe^{II}\mathbf{1}_6][ClO_4]_2$ [space group $P\bar{3}$, $a = 17.5829(3)$ Å, $c = 7.8043(2)$ Å, $\beta = 109.820(3)°$, $T = 295$ K] also possesses Fe1:Fe2 in a 1:2 ratio, and magnetic measurements show a single spin transition at 213 K, indicating that both Fe1 and Fe2 undergo a simultaneous spin transition. $[Fe^{II}\mathbf{1}_6][ClO_4]_2$ slowly decomposes in solutions containing acetic anhydride to form $[Fe^{III}_3O(OAc)_6\mathbf{1}_3][ClO_4]$ [space group $I2$, $a = 10.1547(7)$ Å, $b = 16.5497(11)$ Å, $c = 10.3205(9)$ Å, $\beta = 109.820(3)°$, $T = 200$ K]. The isosceles Fe_3 unit contains two Fe···Fe distances of 3.2844(1) Å and a third Fe···Fe distance of 3.2857(1) Å. The magnetic data can be fit to a trinuclear model with $\mathscr{H} = -2J(S_1 \cdot S_2 + S_2 \cdot S_3) - 2J_{13}(S_1 \cdot S_3)$, where $J = -27.1$ and $J_{13} = -32.5$ cm^{-1}.

Introduction

Some hexacoordinate Fe(II) complexes exhibit a transition from a low $S = 0$ (LS) to a high spin $S = 2$ (HS) with increasing temperature. A few Fe^{II}-based spin-crossover materials have a two-step spin transition attributed to two different spin-crossover sites, each undergoing a transition at different temperatures.[1] We have revisited the homoleptic Fe(II) isoxazole complexes[2] with the goal of developing new Fe(II) spin-crossover materials. Isoxazole (**1**) can act as a monodentate ligand able to coordinate to a metal via either N or O. The previously reported magnetic properties[2] for $[Fe^{II}\mathbf{1}_6][ClO_4]_2$ and $[Fe^{II}\mathbf{1}_6][BF_4]_2$ reveal spin-crossover behavior. $[Fe^{II}\mathbf{1}_6][ClO_4]_2$ was reported to undergo a single spin transition at 212.5 K, having a room-temperature magnetic moment, $\mu_{eff}(T)$, of 5.28 μ_B and a moment of 1.3 μ_B below 180 K, consistent with residual paramagnetism.

$[Fe^{II}\mathbf{1}_6][BF_4]_2$ was reported to exhibit an unusual temperature dependence of the magnetic moment with a 5.25 μ_B room-temperature moment, as expected for HS Fe(II), and 1.90 μ_B below 70 K representing 13% residual HS Fe(II) paramagnetism.[2] Unexpectedly, however, an intermediate moment of 3.30 μ_B was observed between 110 and 150 K. This anomaly was initially attributed to an impurity,[2] but is herein shown not to be the case. Whereas we recently reported the magnetic properties and the HS structure of $[Fe^{II}\mathbf{1}_6][BF_4]_2$[3] with *N*-bonded **1**, herein we report an improved refinement of the HS structure of $[Fe^{II}\mathbf{1}_6][BF_4]_2$ in addition to its 130 K mixed HS/LS structure and the 295 K structure of $[Fe^{II}\mathbf{1}_6][ClO_4]_2$. These structures enabled the identification of the transition temperatures associated with

* Author to whom correspondence should be addressed. E-mail: jsmiller@chem.utah.edu.

† Present address: Institute for Inorganic and Analytical Chemistry, Johannes-Gutenberg University, Mainz, Germany.

(1) Gütlich, P.; Hauser, A.; Spiering, H. *Angew. Chem., Int. Ed. Engl.* **1994**, *33*, 2024. König, E. *Prog. Inorg. Chem.* **1987**, *35*, 527.

(2) Driessen, W. L.; van der Voort, P. H. *Inorg. Chim. Acta* **1977**, *21*, 217.

(3) Hibbs, W. H.; Arif, A. M.; van Koningsbruggen, P. J.; Miller, J. S. *CrystEngComm* **1999**, 4.

10.1021/ic034226p CCC: $25.00
Published on Web 08/05/2003

each Fe(II) site. Furthermore, in the presence of acetic anhydride the $[ClO_4]^-$ salt decomposes in solution to $[Fe^{III}{}_3O(OAc)_6\mathbf{1}_3][ClO_4]$, whose structure and magnetic behavior are reported.

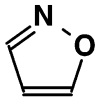

Isoxazole, **1**

Experimental Section

General. Isoxazole (Acros, 99%), $Fe[BF_4]_2 \cdot 6H_2O$ (Aldrich, 97%), $Fe[ClO_4]_2 \cdot 6H_2O$ (GFS Chemical Co.), $Fe[ClO_4]_3 \cdot 6H_2O$ (GFS Chemical Co), sodium acetate (Mallinckrodt), and acetic anhydride (Fisher Scientific) and solvents were used without any further purification. *Perchlorate materials were kept wet as a precaution against explosion as anhydrous perchlorates are prone to detonation when subjected to scraping*.

$[Fe\mathbf{1}_6][BF_4]_2$ and **$[Fe\mathbf{1}_6][ClO_4]_2$** were prepared according to the literature[2] using 69.0 mg (1.00 mmol) isoxazole, 42.2 mg and 45.4 mg (0.125 mmol) of the Fe(II) salt, respectively, 3 mL of nitromethane, and 2 mL of acetic anhydride. Crystallization occurred at low temperature (10 to −20 °C) or by slow diffusion of diethyl ether. The iron perchlorate−isoxazole solution placed in the 10 °C bath cocrystallized small pale pink crystals and small red crystals. The pale pink crystals proved to be $[Fe\mathbf{1}_6][ClO_4]_2$ and analysis of the red crystals revealed a structure of $[Fe_3O(OAc)_6\mathbf{1}_3][ClO_4]$. After 6 months undisturbed, crystals of $[Fe\mathbf{1}_6][BF_4]_2$ grew into mm-sized prisms and the crystals of $[Fe\mathbf{1}_6][ClO_4]_2$ remained small and opaque. IR (cm^{-1}) $[Fe\mathbf{1}_6][BF_4]_2$: 943 (m), 874 (m). IR (cm^{-1}) $[Fe\mathbf{1}_6][ClO_4]_2$: 1039 (s), 945 (m), 874 (m). IR (cm^{-1}) $[Fe_3O(OAc)_6\mathbf{1}_3][ClO_4]$: 1227 (s), 1145 (s), 1095 (s), 1052 (s), 955 (s), 895 (m). DSC $[Fe\mathbf{1}_6][BF_4]_2$: 198 K. DSC $[Fe\mathbf{1}_6][ClO_4]_2$: 206 K (cooling), 215 K (heating).

$[Fe_3O(OAc)_6\mathbf{1}_3][ClO_4]$ was prepared from 45.4 mg (0.125 mmol) of the $Fe[ClO_4]_2 \cdot 6H_2O$ in a solution of 3 mL of nitromethane and 2 mL of acetic acid. Small red/orange crystalline $[Fe_3O(OAc)_6(OH_2)_3][ClO_4]$ was isolated and dried under vacuum thermolysis (150 °C). The dehydrated material was redissolved in minimal **1** and formed $[Fe_3O(OAc)_6\mathbf{1}_3][ClO_4]$ from slow evaporation. Alternatively, $[Fe_3O(OAc)_6(OH_2)_3][ClO_4]$ was prepared according to the previously reported[4] method from 1.64 mg (20.0 mmol) of $Fe[ClO_4]_3 \cdot 6H_2O$ and 4.62 mg (10.0 mmol) of sodium acetate. As before, the red/orange crystalline material was then collected and dehydrated and finally redissolved in minimal isoxazole.

Physical Methods. The 2 to 300 K magnetic susceptibility was determined on a Quantum Design MPMS-5XL 5 T SQUID as previously described.[5] In addition to correcting for the diamagnetic contribution from the sample holder, core diamagnetic corrections of −13, −36.0, −32.0, −32.2, and -30×10^{-6} emu/mol were used for Fe^{II}, **1**, $[ClO_4]^-$, $[BF_4]^-$, and $[OAc]^-$, respectively. Differential scanning calorimetry (DSC) was performed on a TA Instruments model 2910 DSC equipped with a LNCA liquid N_2 cooling accessory enabling operation between −150 and 500 °C at 10 °C/min. Infrared spectra (600−4000 ± 2 cm^{-1}) were obtained on a Bio-Rad FT-40 spectrophotometer in mineral-oil mulls.

X-ray Structure Determination. A pale pink, single crystal of $[Fe\mathbf{1}_6][BF_4]_2$ was cut down (0.35 × 0.35 × 0.35 mm) and coated with traces of viscous oil before it was mounted on a glass fiber. The unit cell was determined at 130 K from 10 images exposed for 20 s on a Nonius Kappa CCD diffractometer equipped with Mo Kα radiation ($\lambda = 0.71073$ Å). Indexing and unit cell refinement based on all observed reflections from those 10 frames indicated triclinic $P\bar{1}$. After complete data collection, the crystal was warmed to 192 K for unit cell determination; however, an accurate refinement was not possible due to a high degree of disorder introduced during the transition region. The crystal was then warmed to 260 K and subsequent indexing and unit cell refinement based on all observed reflections from those 10 frames indicated trigonal $P\bar{3}$. Equivalent reflections were merged and only those for which $I_o > 2\sigma(I)$ were included in the refinement, where $\sigma(F_o)^2$ is the standard deviation based on counting statistics. Reflections were indexed, integrated, and corrected for Lorentz, polarization, and absorption effects using DENZO-SMN and SCALEPAC.[6] The structure was solved by a combination of direct and heavy atom methods using SIR 97.[7] All of the nonhydrogen atoms were refined with anisotropic displacement coefficients. Hydrogen atoms of Fe2, 260 K, were assigned isotropic displacement coefficients U(H) = 1.2U(C) and their coordinates were allowed to ride on their respective carbons using SHELXL97.[8] All other hydrogen atoms were located and refined isotropically. The final cycle of full-matrix least-squares refinement of $[Fe\mathbf{1}_6][BF_4]_2$ at 130 K was based on 7444 observed reflections [$I_o > 2\sigma(I)$] and converged with unweighted and weighted agreement factors $R(F) = 0.0328$ and $wR(F^2) = 0.0734$, respectively.[9] There is one rotationally disordered anion in the unit cell. A summary of the crystallographic data is presented in Table 1.

The final cycle of full-matrix least-squares refinement of $[Fe\mathbf{1}_6][BF_4]_2$ at 260 K was based on 2240 observed reflections [$I_o > 2\sigma(I)$] and converged with unweighted and weighted agreement factors $R(F) = 0.0496$ and $wR(F^2) = 0.1296$, respectively.[9] There is one rotationally disordered anion in the unit cell. The six isoxazole ligands of Fe2 are disordered such that each ring occupies two positions related by ∼30° rotation around the Fe−N axis. A summary of the crystallographic data is presented in Table 1.

Cell constants and an orientation matrix for the data collection were obtained for a pale purple crystal of $[Fe^{II}\mathbf{1}_6][ClO_4]_2$ (0.28 × 0.26 × 0.24 mm) from 10 images exposed for 20 s at 150, 235, and 295 K on a Nonius Kappa CCD diffractometer. Indexing and unit cell refinement based on all observed reflections from those 10 frames indicated a trigonal $P\bar{3}$ lattice at all temperatures. The structure was determined at 295 K, as cracking within the crystal occurred below 250 K and made the structure determination at low temperature impossible. The structure was solved by a combination of direct and heavy atom methods using SIR 97.[7] The nonhydrogen atoms were refined with anisotropic displacement coefficients. Hydrogen atoms were assigned isotropic displacement coefficients U(H) = 1.2U(C), and their coordinates were allowed to ride on their respective carbons. The final cycle of full-matrix least-squares refinement was based on 4841 observed reflections [$I_o > 2.00\sigma(I)$] and 187 parameters and converged with unweighted and weighted

(4) Johnson, M. K.; Powell, D. B.; Cannon, R. D. *Spectrochim. Acta, Part A* **1981**, *37A*, 995.
(5) Brandon, E. J.; Rittenberg, D. K.; Arif, A. M.; Miller, J. S. *Inorg. Chem.* **1998**, *37*, 3376.
(6) Otwinowski, Z.; Minor, W. Processing of X-ray Diffraction Data Collected in Oscillation Mode. *Methods Enzymol.* **1997**, *276*, 307−326.
(7) Altomare, A.; Burla, M. C.; Camalli, M.; Cascarano, G.; Giacovazzo, C.; Guagliardi, A.; Moliteni, A. G. G.; Polidori, G.; Spagna, R. SIR97 (Release 1.02) − A Program for Automatic Solution and Refinement of Crystal Structure. *J. Appl. Crystallogr.* **1999**, *32*, 115.
(8) Sheldrick, G. M. SHELX97 [Includes SHELXS97, SHELXL97, CIFTAB] − Programs for Crystal Structure Analysis (Release 97-2); University of Göttingen: Germany, 1997.
(9) $R1 = \sum(||F_o| - |F_c||)/\sum|F_o|$, $wR^2 = [\sum(w(F_o^2 - F_c^2)^2)/\sum(F_o^2)^2]^{1/2}$, and S = goodness-of-fit on $F^2 = [\sum(w(F_o^2 - F_c^2)^2/(n-p)]^{1/2}$, where n is the number of reflections and p is the number of parameters refined.

Table 1. Summary of the Crystallographic Data for $[Fe^{II}\mathbf{1}_6][BF_4]_2$, $[Fe^{II}\mathbf{1}_6][ClO_4]_2$, and $[Fe^{III}_3O(OAc)_6\mathbf{1}_3][ClO_4]$

	$[Fe\mathbf{1}_6][BF_4]_2$		$[Fe\mathbf{1}_6][ClO_4]_2$	$[Fe^{III}_3O(OAc)_6\mathbf{1}_3][ClO_4]$
formula	$C_{18}H_{18}B_2F_8FeN_6O_6$		$C_{18}H_{18}Cl_2FeN_6O_{14}$	$C_{21}H_{27}ClFe_3N_3O_{20}$
formula weight	643.85		669.14	844.46
temperature, K	260(1)	130(1)	295(1)	200(1)
space group	$P\bar{3}$	$P\bar{1}$	$P\bar{3}$	$I2$
a, Å	17.4387(4)	7.5413(1)	17.5829(3)	10.1547(7)
b, Å	17.4387(4)	16.7481(2)	17.5829(3)	16.5497(11)
c, Å	7.6847(2)	17.0901(2)	7.8043(2)	10.3205(9)
α, deg	90	117.8195(8)	90	90
β, deg	90	91.5231(6)	90	109.820(3)
γ, deg	120	90.5309(6)	120	90
Z	3	3	3	2
V, Å^3	2023.88(8)	1900.96(4)	2089.51(7)	1631.7(2)
μ, mm^{-1}	0.659	0.702	0.809	1.485
ρ_{calcd}, g cm^{-3}	1.585	1.687	1.595	1.719
R(F)[a]	0.0496	0.0328	0.0886	0.0405
$R_w(F^2)$[b]	0.1296	0.0734	0.2555	0.1006
λ, Å	0.71073	0.71073	0.71073	0.71073

[a] $\sum(|F_o| - |F_c|)/\sum|F_o|$. [b] $\{\sum w[F_o^2 - F_c^2]^2/\sum w[F_o^2]^2\}^{1/2}$.

agreement factors R(F) = 0.0886 and wR(F^2) = 0.2555, respectively. The high R values are a consequence of crystal quality rather than the presence of disorder. A summary of the crystallographic data is presented in Table 1.

Cell constants and orientation matrix for data collection for red $[Fe_3O(OAc)_6\mathbf{1}_3][ClO_4]$ (0.24 × 0.23 × 0.21 mm) were obtained from 10 images exposed for 20 s at 200 K on a Nonius Kappa CCD diffractometer. The systematic absences uniquely determine the space group of *I2*. The structure was solved by a combination of direct and heavy atom methods using SIR 97.[7] The nonhydrogen atoms were refined with anisotropic displacement coefficients. Hydrogen atoms were assigned isotropic displacement coefficients U(H) = 1.2U(C), and their coordinates were allowed to ride on their respective carbons. The final cycle of full-matrix least-squares refinement for $[Fe_3O(OAc)_6\mathbf{1}_3][ClO_4]$ was based on 2402 observed reflections [$I_o > 2.00\sigma(I)$] and 225 parameters and converged with unweighted and weighted agreement factors, R(F) = 0.0405 and wR(F^2) = 0.1006, respectively.[9] Because of the imposed 2-fold C_2 symmetry on the N(1)-containing isoxazole ligand, the oxygen (O7c) and opposite carbon atom exhibit disorder; hence, oxygen was refined with 0.875. Refinement began with a 0.50 occupancy; however, based on residual electron density in the Fourier map there is an indication of greater electronegativity in this area requiring a 0.875 refinement value. The $[ClO_4]^-$ is disordered due to the imposed 2-fold symmetry. The oxygen atoms O(11) and O(12) were refined with 75% occupancy. O(10), which also sits on the 2-fold axis, was refined with 50% occupancy. There is no crystallographic symmetry imposed on the anions. A summary of the crystallographic data is presented in Table 1.

Results and Discussion

Synthesis. $[Fe\mathbf{1}_6]X_2$ {X = $[BF_4]^-$, $[ClO_4]^-$} was prepared by the addition of isoxazole to a solution of $FeX_2 \cdot xH_2O$ in an 8:1 ratio. Nitromethane and acetic anhydride were chosen as solvents to prevent water coordination to the Fe(II). These complexes are deliquescent at room temperature. Product formation occurred overnight upon slow diffusion with diethyl ether; however, crystals suitable for X-ray analysis required slow growth at 10 °C. Crystals grown below 0 °C formed too rapidly and produced cracked crystals that were not suitable for X-ray analysis. As expected, the high-spin Fe(II) materials are essentially colorless at room temperature. As the temperature is reduced, the crystals appear pink and eventually become purple near −50 °C. The purple color continues to intensify and darken with decreasing temperature, consistent with the increasing concentration of low-spin Fe(II). A variety of solvents were utilized; however, protic solvents such as water or methanol were not suitable because of their preferential coordination to iron. The Fe(II) salts are insoluble in most other solvents.

The synthesis of $[Fe\mathbf{1}_6][ClO_4]_2$ yielded a coproduct that, upon X-ray analysis, proved to be the previously unknown Fe(III) oxo-trimer compound $[Fe_3O(OAc)_6\mathbf{1}_3][ClO_4]$. The formation of the coproduct can be controlled based on the quality of acetic anhydride. Over time the acetic anhydride hydrolyzes and forms acetic acid, and under this condition Fe(II) is oxidized to Fe(III) and the formation of the Fe(III) trimer occurs. Adding 2 mL of acetic acid to the reaction solution verified this observation. This produced a substantial increase in the formation of the Fe(III) trimer, yet without 100% formation. Subsequently, acetic anhydride was wholly replaced by acetic acid in the reaction. Small red-orange crystalline material was isolated; however, infrared analysis indicated formation of $[Fe_3O(OAc)_6(OH_2)_3][ClO_4]$. The sample was successfully dehydrated under vacuum thermolysis (150 °C) and then redissolved in minimal **1**, subsequently forming $[Fe_3O(OAc)_6\mathbf{1}_3][ClO_4]$ upon slow evaporation. The Fe(III) trimer was also prepared according to the reported synthesis of various $[Fe_3O(OAc)_6L_3]X$ {L = H_2O, pyridine, γ-picoline; X = $[NO_3]^-$, $[ClO_4]^-$}.[4] This method first requires the synthesis of $[Fe^{III}_3O(OAc)_6(OH_2)_3][ClO_4]$ from $Fe^{III}[ClO_4]_3$ hydrate and sodium acetate. The red-orange $[Fe_3O(OAc)_6(OH_2)_3][ClO_4]$ crystals were then collected and redissolved in minimal **1** and cooled to 5 °C resulting in formation of $[Fe_3O(OAc)_6\mathbf{1}_3][ClO_4]$.

Structure. $[Fe\mathbf{1}_6][ClO_4]_2$. The unit cell of $[Fe^{II}\mathbf{1}_6][ClO_4]_2$ at 295 K contains three Fe(II) ions while the asymmetric unit contains two in a 1:2 ratio; the first one possesses Fe1 and sits on the inversion center and lies on the C_3 axis, while the second possesses Fe2 (in a 1:2 ratio) and sits on a 3-fold symmetry site without an inversion center. The symmetry related Fe2′ is generated through the inversion center located on Fe1 (Figure 1a). An ORTEP atom-labeling diagram of both crystallographically independent $[Fe^{II}\mathbf{1}_6]^{2+}$'s shows Fe(II) octahedrally coordinated by *N*-bound **1** (Figure 1b).

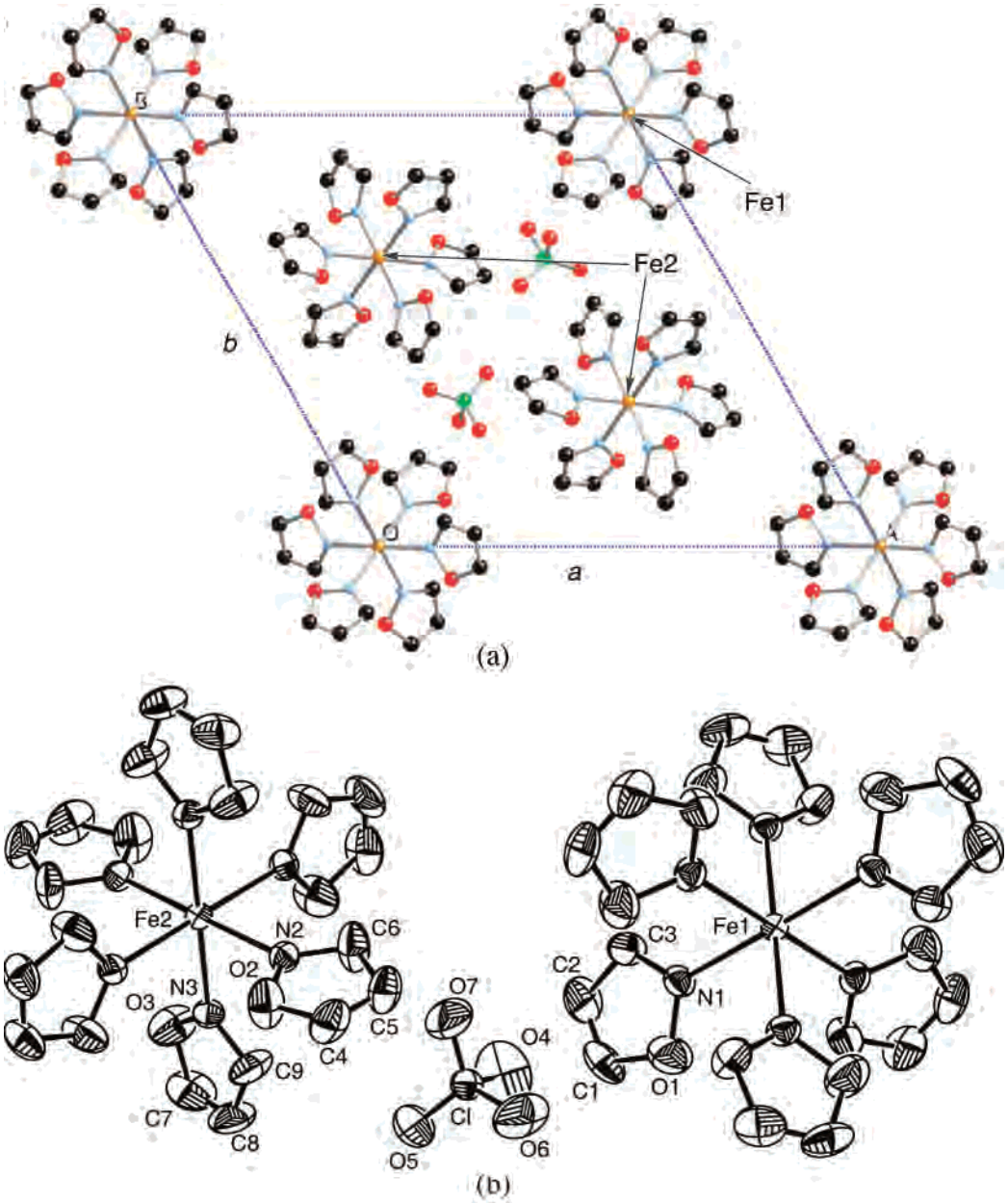

Figure 1. Part of the unit cell of $[Fe^{II}\mathbf{1}_6][ClO_4]_2$ at 295 K. Fe1 sits on the inversion center and lies on the C_3 axis, whereas Fe2 lacks an inversion center but sits on a 3-fold symmetry site, and the symmetry related Fe2′ is generated through the inversion center located on Fe1. The unit cell of $[Fe\mathbf{1}_6][BF_4]_2$ at 260 K is the same, however, there is disorder of the isoxazole ligands on Fe2 and the $[BF_4]^-$ has been omitted for clarity. At 130 K the unit cell of $[Fe\mathbf{1}_6][BF_4]_2$ has Fe1 siting on $P\bar{1}$ at each vertex and Fe2 sits in the center of the unit cell with imposed symmetry, and the $[BF_4]^-$ is disordered (a). ORTEP (40% electron density) of $[Fe^{II}\mathbf{1}_6][ClO_4]_2$ (b). The crystallographically unique atoms are labeled. H atoms have been omitted for clarity. Fe(II) is octahedrally coordinated by *N*-bound **1** with an average Fe−N distance of 2.170 Å (b).

There is no crystallographic symmetry imposed on the anions. The Fe−N distances average 2.171 and 2.175 Å for Fe1 and Fe2, respectively (Table 2). The isoxazole bond distances are essentially as reported[10] for the free ligand. All molecules in the unit cell have a paddle-wheel configuration of the ligands, such that oxygen atoms on the isoxazole rings point in the same direction with an average neighboring ligand O···O separation of 5.04 Å. The lack of high quality crystals made data collection at lower temperatures difficult. However, enough information was available at 235 and 150 K to indicate the $P\bar{3}$ space group is maintained throughout the temperature region.

$[Fe\mathbf{1}_6][BF_4]_2$. As occurs for $[Fe^{II}\mathbf{1}_6][ClO_4]_2$, the unit cell of $[Fe\mathbf{1}_6][BF_4]_2$ at both 260 and 130 K contains three molecules and two unique iron sites (Figure 2), Fe1 and Fe2, in a 1:2 ratio. At 260 K Fe1 and Fe2 occupy the unit cell in a 1:2 ratio and Fe1 and Fe2 have the same symmetry as that discussed above for $[Fe^{II}\mathbf{1}_6][ClO_4]_2$. ORTEP atom-labeling diagrams of the cation of $[Fe\mathbf{1}_6][BF_4]_2$ at 260 and 130 K show Fe(II) octahedrally coordinated by *N*-bound **1** at both temperatures (Figure 2). The isoxazole bond distances are essentially as reported[10] for the free ligand.

Upon cooling to 130 K, the Fe1-containing cation undergoes a reduction in symmetry and contains three crystallographically independent ligands with the remaining three

(10) Borello, E. *Corsi Semin. Chim.* **1968**, *14*, 72.

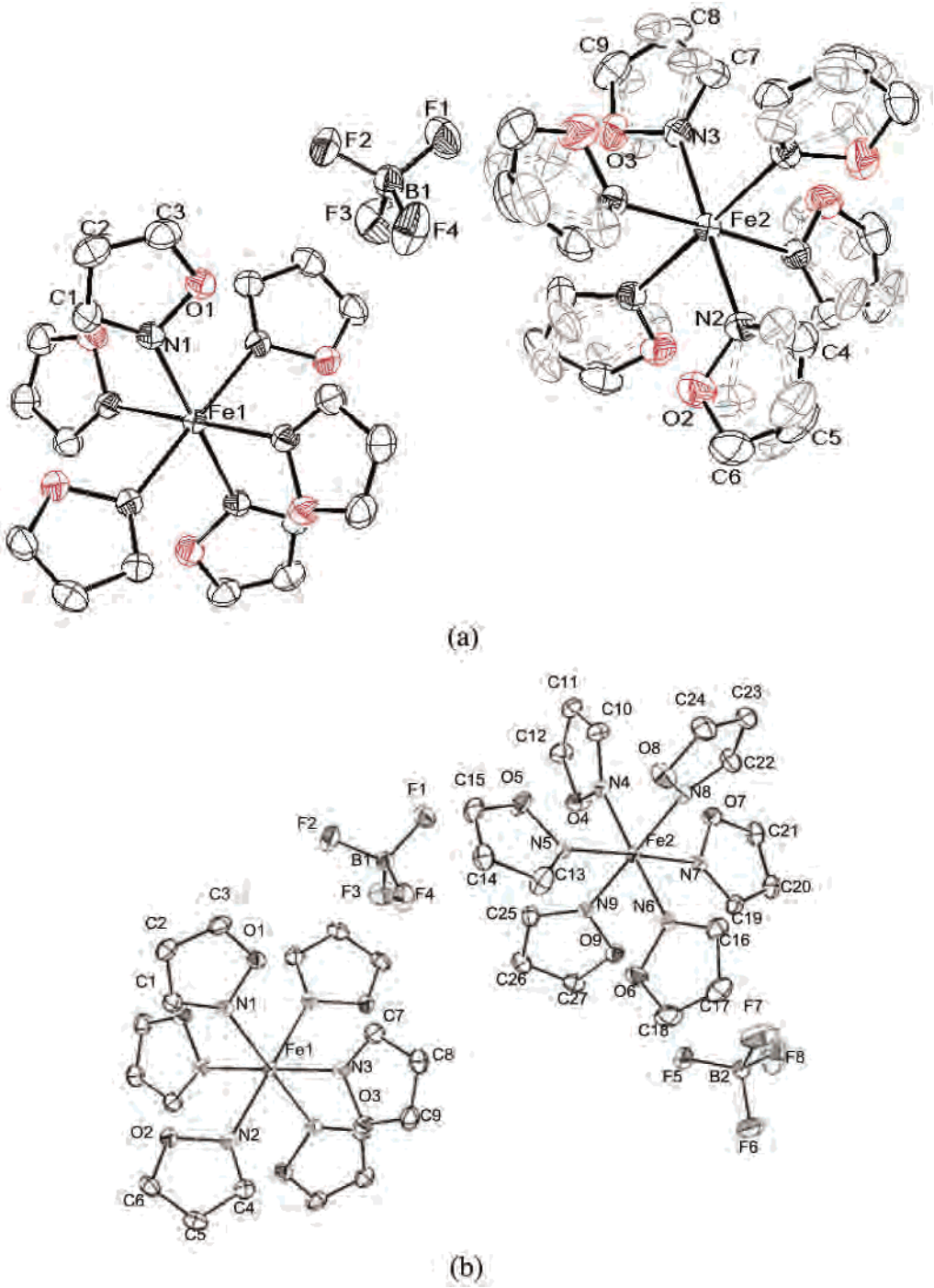

Figure 2. ORTEP drawings of $[Fe\mathbf{1}_6][BF_4]_2$ at (a) 260 K (30% electron density) and (b) 130 K (30% electron density). The six isoxazole ligands of Fe2 at 260 K are shown disordered, occupying two positions (solid and dashed bonds) related by ~30° rotation around the Fe−N axis. H atoms have been omitted for clarity. Crystallographically unique atoms are labeled.

generated through a center of inversion (Figure 3b). The same paddle-wheel configuration is maintained with neighboring ligand O···O separations ranging from 4.035 to 4.087 Å, averaging 4.044 Å.

The Fe2-containing cation is not located on any symmetry element and contains six crystallographically independent ligands with mixed orientations. Two neighboring ligand pairs have oxygen atoms pointing toward each other with O···O separations of 2.912 and 3.582 Å. The remaining ligand pair attempts a paddle-wheel configuration with a larger O···O separation of 4.632 Å. Assignment of the O and C atoms in the crystallographic refinement was performed with thorough examination of electron densities and N−O, O−C, C−C, and N−C bond distances of the ligand. The requirements of bond distances and electron densities were satisfied only with this unusual mixed orientation of the ligands. Additionally, the *trans*-ligand dihedral angles increase at reduced temperature. At 260 K, the three *trans*-isoxazole ligand pairs form dihedral angles of less than 2°. At 130 K, the *trans*-isoxazole dihedral angles increase and are 18°, 38°, and 46°. The largest angle is the one associated with the paddle-wheel ligand pair isoxazole.

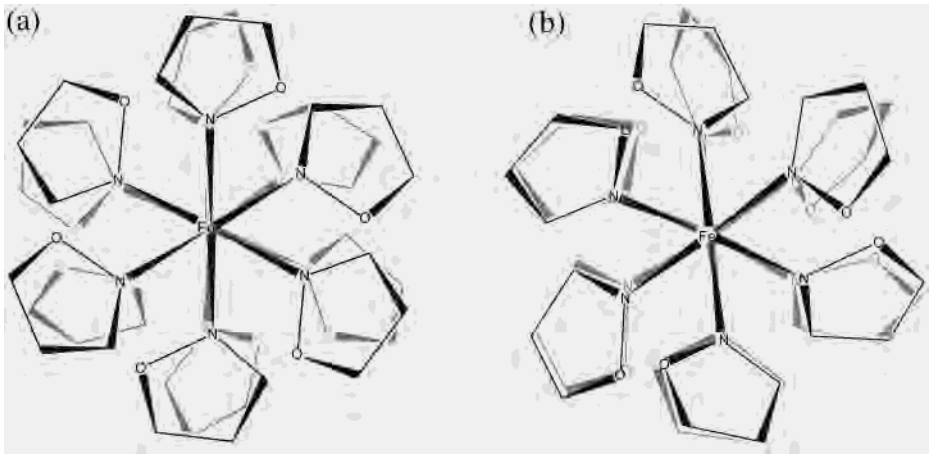

Figure 3. Comparison between cations containing Fe1 (black) and Fe2 (gray) for $[Fe\mathbf{1}_6][BF_4]_2$ at 260 K (a); and comparison of cations containing Fe2 of $[Fe\mathbf{1}_6][BF_4]_2$ at 260 (black) and 130 K (gray) showing one orientationally rotated isoxazole ligand (b).

Table 2. List of Key Fe−N Bond Distances for $[Fe\mathbf{1}_6][BF_4]_2$ and $[Fe\mathbf{1}_6][ClO_4]_2$

	$[Fe\mathbf{1}_6][ClO_4]_2$	$[Fe\mathbf{1}_6][BF_4]_2$	
temperature, K	295	260	130
Fe1−N, Å	2.171(3)	2.182(2)	2.1716(14) 2.1678(14) 2.1688(14)
average Fe1−N, Å	2.171	2.182	2.1694
Fe2−N Å	2.173(3) 2.176(3)	2.170(2) 2.176(2)	1.9651(14) 1.9710(14) 1.9720(14) 1.9762(13) 1.9848(14) 1.9901(14)
average Fe2−N, Å	2.175	2.173	1.9765

Fe1−N distances average 2.182 and 2.169 Å at 260 and 130 K, respectively, and are typical of Fe−N distances reported for high-spin Fe(II)[2] (Table 2). The Fe−N bond shortening is due to contraction arising from a decreased temperature. The average Fe2−N distances are 2.173 and 1.977 Å at 260 and 130 K, respectively. This represents a 9% contraction of the Fe−N bond with the shorter bond distance being typical for low-spin Fe(II). The overall unit cell volume contraction is 6%.

$[Fe_3O(OAc)_6\mathbf{1}_3][ClO_4]$. The ORTEP of $[Fe_3O(OAc)_6\mathbf{1}_3][ClO_4]$ shows an μ_3-oxo-bridged trinuclear complex (Figure 4). The unit cell contains two molecules with 2-fold crystallographic symmetry imposed on each molecule with the atoms O(9), Fe(2), and N(1) sitting on the 2-fold axis. Figure 4 shows the 87.5% preferred orientation of the N(1)-containing isoxazole ligand that is disordered due to the imposed symmetry. The isoxazole bond distances are essentially as reported[10] for the free ligand. The three irons form an isosceles triangle that is very nearly an equilateral triangle having Fe···Fe distances of 3.2857(1) and 3.2844(1) Å and Fe−N distances of 2.187 and 2.185 Å. Other reported oxo-trinuclear iron (III) compounds have Fe···Fe distances ranging from 3.289 to 3.317 Å and Fe−N distances ranging from to 2.162 to 2.226 Å.[11]

Magnetic Properties. The magnetic susceptibilities, $\chi(T)$, of $[Fe\mathbf{1}_6][BF_4]_2$, $[Fe^{II}\mathbf{1}_6][ClO_4]_2$, and $[Fe_3O(OAc)_6\mathbf{1}_3][ClO_4]$ were measured between 5 and 300 K and do not exhibit a linear $\mu_{eff}(T)$ $[\equiv(8\chi T)^{1/2}]$; hence they do not obey the Curie−Weiss expression. $[Fe^{II}\mathbf{1}_6][ClO_4]_2$ has a moment of 5.1 μ_B at 270 K, which remains fairly constant with decreasing temperature until ∼240 K. Below ∼240 K the moment drops more rapidly until ∼180 K where it plateaus to a moment of ∼1.9 μ_B and is consistent with 18% of the cations remaining in the high-spin state until the moment ultimately approaches 0.8 μ_B below 10 K (Figure 5). The low temperature behavior is unusual, i.e., cooling at low temperature shows a considerably smaller μ_{eff} compared to that observed upon heating at the same temperatures, but are reproducible and consistent with the ^{57}Fe Mössbauer spectroscopy.[12] The abrupt drop in $\mu_{eff}(T)$ has a maximum in $d\mu_{eff}(T)/dT$ or spin-

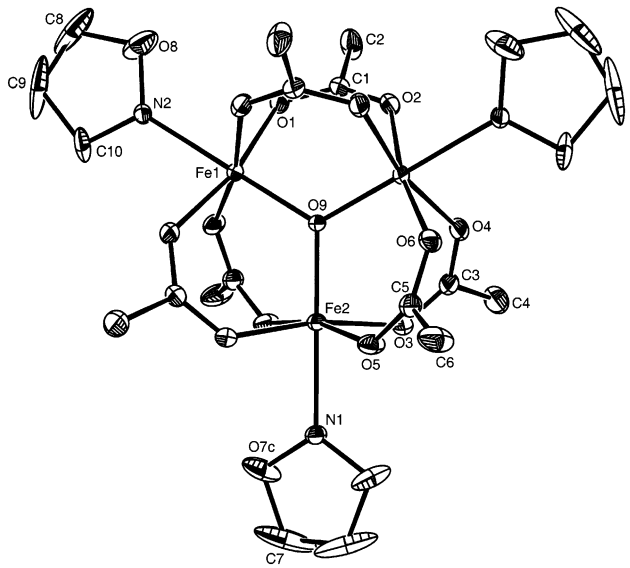

Figure 4. ORTEP (30% electron density) of $[Fe_3O(OAc)_6\mathbf{1}_3][ClO_4]$ (30% electron density). The crystallographically unique atoms are labeled. H atoms have been omitted for clarity.

(11) (a) Cui, Y.; Wang, Y.-M.; Zheng, Y.; Zhou, W.-B.; He, L.-J.; Cai, S.-H.; Chen, B.; Zhang, L.-N. *Chinese J. Struct. Chem.* **1999**, *18*, 51. (b) Bond, A. M.; Clark R. J. H.; Humphrey D. G.; Panayiotopoulos P.; Skelton B. W.; White A. H. *J. Chem. Soc., Dalton Trans.* **1998**, 1845. (c) Sowrey, F. E.; Tilford, C.; Wocadlo, S.; Anson, C. E.; Powell, A. K.; Bennington, S. M.; Montfrooij, W.; Jayasooriya, U. A.; Cannon, R. D. *J. Chem. Soc., Dalton Trans.* **2001**, 862. (d) Wu, R.; Poyraz, M.; Sowrey, F. E.; Anson, C. E.; Wocadlo, S.; Powell, A. K.; Jayasooriya, U. A.; Cannon, R. D.; Nakamoto, T.; Katada, M.; Sano, H. *Inorg. Chem.* **1998**, *37*, 1913.

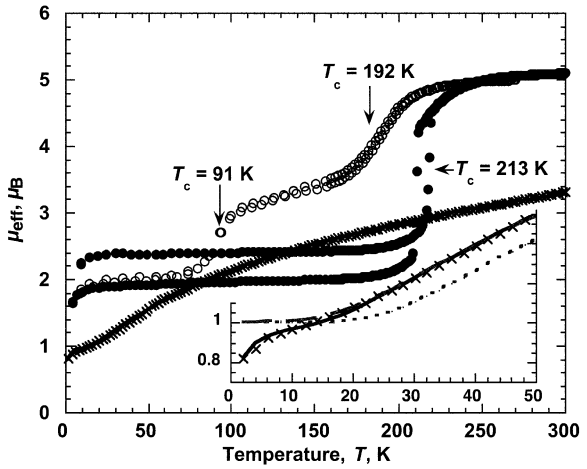

Figure 5. $\mu_{eff}(T)$ for $[Fe^{III}_3O(OAc)_6\mathbf{1}_3][ClO_4]$ [μ_{eff}(300 K) = 3.34 μ_B] (×), $[Fe^{II}\mathbf{1}_6][ClO_4]_2$ [μ_{eff}(300 K) = 5.1 μ_B (calculated value for g = 2, d^6 high-spin Fe(II) is 4.90 μ_B] (●), and $[Fe^{II}\mathbf{1}_6][BF_4]_2$ [μ_{eff}(300 K) = 5.0 μ_B (calculated value for g = 2, d^6 high-spin Fe(II) is 4.90 μ_B] (○). Spin transitions occurs at 213 K (cooling) and 222 K (warming) as determined by the maxima in $d\mu_{eff}(T)/dT$ for $[Fe\mathbf{1}_6][ClO_4]_2$. A moment of 3.3 μ_B is observed at the plateau (130 K). Below ~70 K, μ_{eff} ~1.8 μ_B indicating residual paramagnetism for $[Fe\mathbf{1}_6][BF_4]_2$. Spin transitions occur at 192 and 91 K as determined by the maxima in $d\mu_{eff}(T)/dT$. The solid line is the fit of $\mu_{eff}(T)$ for $[Fe_3O(OAc)_6\mathbf{1}_3][ClO_4]$ to a trinuclear model using eq 7, with J = −32.5 cm^{-1}, J_{13} = −27.1 cm^{-1}, g = 2.00, and TIP = 300 × 10^{-6} emu/mol Fe(III), and intertrimer coupling zJ' of −4.2 cm^{-1}. The inset shows the low-temperature region (T < 50 K), as well as the fit to an equilateral triangular model (- - -; J = −29.4 cm^{-1} (J_{13} = J; zJ' = 0), g = 2.00, and TIP being zero, and an isosceles triangular model (—; J = −34.3 cm^{-1}; J_{13} = −28.7 cm^{-1}; zJ' = 0), g = 2.00, and TIP = 300 × 10^{-6} emu/mol Fe(III).

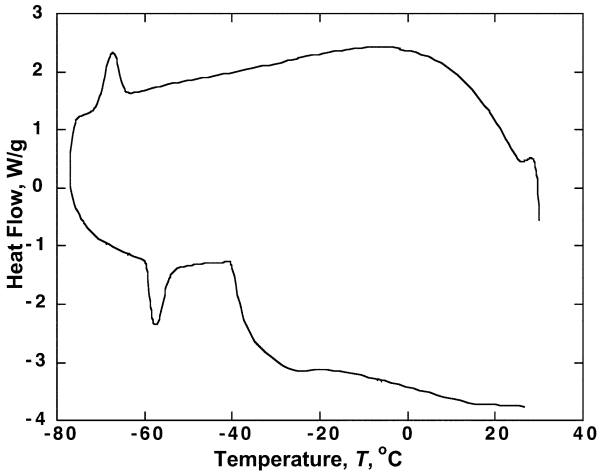

Figure 6. Specific heat (DSC) of $[Fe\mathbf{1}_6][ClO_4]_2$ with observed phase transitions at 210 ± 5 K (cooling) and 220 ± 5 K (warming).

crossover transition temperature of 213 K, confirmed by DSC with the observance of a phase transition at 210 ± 5 K (Figure 6). The calculated high-temperature moment, assuming g = 2, for a d^6 high-spin Fe(II) is 4.9 μ_B, which is in accord with the experimental value. Upon warming from 2 K the $\mu_{eff}(T)$ dependence is reversible, and displays hysteresis of 9 K, i.e., 222 K upon warming. DSC confirms the presence of a phase transition upon warming at 220 ± 5 K. This crystal also undergoes a color change from very pale purple to very dark purple as temperature is lowered, consistent with the formation of LS Fe^{II} at low temperature.

Table 3. Comparison of Fe−N Bond Distances (Å) for $[Fe\mathbf{1}_6][BF_4]_2$ and $[Fe\mathbf{1}_6][ClO_4]_2$ with those of Selected Other Spin-Crossover Compounds Structurally Characterized at Two Temperatures

compound	HS (T, K)	HS (T, K)[a]	LS (T, K)
$[Fe\mathbf{1}_6][ClO_4]_2$	2.173(298)		*b*
$[Fe\mathbf{1}_6][BF_4]_2$	2.178(260)	2.169(130)	1.977(130)
[Fe(2-picolylamine)$_3$]Cl$_2$·EtOH [c]	2.195(298)	2.075(115)	2.013(90)
Fe(phen)$_2$(NCS)$_2$ [d]	2.156(293)		1.992(130)
[Fe(btr)$_3$](ClO$_4$)$_2$ [e]	2.163(260)	2.151(190)	1.996(150)
Fe(PM-BiA)$_2$(NCS)$_2$ [f]	2.174(280)		1.956(140)

[a] Measured from the reduced temperature plateau. [b] Not observed. [c] Refs 15b and c. [d] phen = 1,10-phenanthroline. Ref 27. [e] btr = 4,4′-bis-1,2,4-triazole. Ref 14k. [f] PM-BiA = *N*-(2-pyridylmethylene)aminobiphenyl. Ref 15e.

Similarly, $[Fe\mathbf{1}_6][BF_4]_2$ has a moment of 5.0 μ_B at 270 K, which remains fairly constant with decreasing temperature until ~210 K (Figure 5). Between 205 and 170 K, $\mu_{eff}(T)$ drops rapidly and reaches an intermediate plateau having a moment of 3.3 μ_B at 130 K. This plateau is maintained to 115 K followed by a second rapid drop in moment to 2.0 μ_B at 65 K. The magnetic behavior is reproducible and is in agreement with the earlier report.[2] As determined from the maxima in $d\mu_{eff}(T)/dT$, transition temperatures of 192 and 91 K are obtained. Liquid nitrogen cooled DSC shows a peak at 196 ± 5 K confirming a phase transition. The phase transition at 91 K could not be confirmed with DSC due to cooling limitations of the instrument. Upon warming from 2 K the $\mu_{eff}(T)$ dependence is reversible, and displays a hysteresis of <1 K.

The 3.3 μ_B moment at the intermediate plateau is consistent with approximately two-thirds of the Fe(II) having transitioned to a low spin state. Given a low-spin moment of zero, the high-spin molar fraction, X_{HS}, can be calculated by

$$X_{HS} = \mu^2/{\mu_{HS}}^2 \qquad (1)$$

where μ^2 is the moment at the plateau and ${\mu_{HS}}^2$ is the high-temperature moment. From eq 1 X_{HS} is 43%, slightly more than one-third, indicating incomplete transition. The low temperature (<90 K) moment of 1.8 μ_B is reproducible and is consistent with 13%[13] of the iron sites maintaining a high-spin electronic configuration. The high-spin to low-spin transition is also associated with a color change from very pale pink at room temperature to very dark purple upon cooling.

Both $[Fe\mathbf{1}_6][BF_4]_2$ and $[Fe^{II}\mathbf{1}_6][ClO_4]_2$ have Fe−N bond distances in accord with previously reported Fe^{II}−N bond distances according to a high- or low-spin configuration (Tables 2 and 3). Fe−N bond distances of 2.18 ± 0.02 Å are expected for high-spin Fe^{II} and distances of 1.98 ± 0.02 Å are expected for the low-spin configuration.[1] The Fe−N bond shortening results in an overall unit cell volume reduction of 6%. As the compounds are cooled, thermal energy is reduced and all the bond distances contract incrementally including the Fe−N bonds that are most important with respect to the crystal field splittings, Δ_o. When Δ_o exceeds the spin pairing energy arising from double occupancy of an orbital, the LS electron structure becomes

(12) Bhattacharjee, A.; van Koningsbruggen, P. J.; Gütlich, P.; Hibbs, W.; Miller, J. S. in preparation.

(13) Our earlier report (ref 3) of 40% was in error due to a computational mistake.

more stable and leads to further significant shortening of the $Fe^{II}-N$ bonds, which is shown in Tables 2 and 3.

$[Fe\mathbf{1}_6][ClO_4]_2$ exhibits a single spin transition with hysteresis (Figure 5) and at 295 K possesses two iron sites with similar orientations (Figure 1), and apparently there is no crystallographic phase transition. But because of the lack of a crystal structure refinement at low temperature, its Fe−N bond distance changes and volume reduction cannot be determined. In contrast, $[Fe\mathbf{1}_6][BF_4]_2$ exhibits two independent spin transitions that do not exhibit hysteresis. The two-step feature is ascribed the subtle structural differences between the orientational isomers associated with the Fe1 and Fe2 sites of $[Fe\mathbf{1}_6][BF_4]_2$ that lead to slight differences in Δ_o for each site that require different $Fe^{II}-N$ bond contractions in order for that site. Hence, the LS electronic structure of each Fe site is stabilized at different temperatures resulting in the observed two-step spin-crossover behavior. Concurrent examination of the magnetic and crystallographic data shows approximately one-third of the Fe sites remain HS at the plateau, and one-third of the Fe sites have Fe−N bond distances consistent with HS Fe(II). Fe1 and Fe2 can be assigned to the spin transitions at 91 and 192 K, respectively. Detailed discussions regarding the nature of the two-step phenomenon have been previously published.[14]

In addition to the two-step spin-transition behavior, $[Fe\mathbf{1}_6][BF_4]_2$ undergoes a crystallographic phase transition. Crystal structures have been determined for both the HS and LS forms of several spin-transition compounds revealing differences around the FeN_6 core resulting from changes in bond lengths and angles (Table 3).[14k,15] In some cases, more extensive rearrangements resulting in a crystallographic phase transition and a change in space group occur. Prior work concluded that only compounds displaying thermal hysteresis are capable of undergoing a simultaneous crystallography phase transition due to increased cooperative effects within the crystal lattice.[16] However, this correlation is not absolute as shown by $Fe(phen)_2(NCS)_2$, which, despite having a spin transition with hysteresis,[17a] does not undergo a crystallographic phase transition[17b] associated with the spin transition. Spin transitions lacking thermal hysteresis did not, until now, display crystallographic phase transitions, but $[Fe\mathbf{1}_6][BF_4]_2$ is the first example of this. This transition from $P\bar{3}$ high temperature form to the $P\bar{1}$ low temperature form is reversible, but attempts to determine the structure at the intermediate temperature of 192 K could not be refined, presumably because of significant disorder introduced during the transition region. It is probable that $[Fe\mathbf{1}_6][ClO_4]_2$ will not undergo a crystallographic phase transition, as crystallographic data at 295, 235, and 150 K indicate the $P\bar{3}$ space group is maintained throughout the temperature region.

The $\mu_{eff}(T)$ for $[Fe^{III}{}_3O(OAc)_6\mathbf{1}_3][ClO_4]$ does not exhibit either spin-crossover behavior or Curie−Weiss behavior, Figure 5. The room-temperature moment of 3.33 μ_B per Fe^{III} is much lower than the expected value 5.92 μ_B and the moment is 0.88 μ_B per Fe^{III} at 2 K, suggestive of antiferromagnetic coupling. As a consequence of its trinuclear structure the magnetic data was fit to a magnetic model for trinuclear systems.

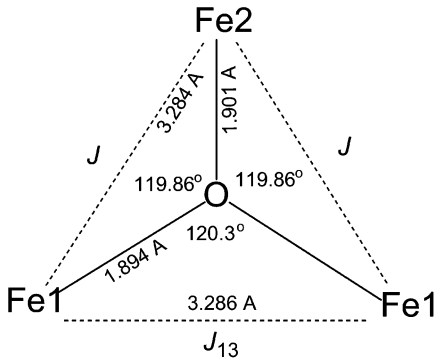

The magnetic properties of $Mn^{III}{}_3(OAc)_6(bipy)_2$, which is structurally and electronically related to $[Fe_3O(OAc)_6\mathbf{1}_3]^+$, was reported, but the fit assumed a linear trinuclear model, i.e., $J_{13} = 0$.[18] Because of the structure, $J_{13} = 0$ was unreasonable, and an equatorial triangular model with $J = J_{13}$ was sought. While an analytical expression for $J = J_{13}$ was reported,[19] none could be found for $J \neq J_{13}$. $[Fe_3O(OAc)_6\mathbf{1}_3]^+$ has an isosceles triangular arrangement of Fe^{III} ions, a model accounting for $J \neq J_{13}$, i.e., using the Hamiltonian $\mathscr{H}$

$$\mathscr{H} = -2J(S_1 \cdot S_2 + S_2 \cdot S_3) - 2J_{13}(S_1 \cdot S_3) \qquad (2)$$

(S_{13} is the vectorized sum defined as $|S_1 - S_3| \leq S_{13} \leq S_1 + S_3$ and S_T is the vectorized sum defined as $|S_{13} - S_2| \leq S_T < S_{13} + S_2$) was developed to analyze the susceptibility. The eigenvalues for $\mathscr{H}$ are given by

$$E(S_T, S_{13}) = -J[S_T(S_T + 1) - S_{13}(S_{13} + 1)] - J_{13}[S_{13}(S_{13}+1)] \qquad (3)$$

and are supplied as Supporting Information.The spin Hamiltonian for the trimer, $\mathscr{H}_{trimer}$, taking into account the Zeeman

(14) (a) Köppen, H.; Müller, E. W.; Köhler, C. P.; Spiering, H.; Meissner, E.; Gütlich, P. *Chem. Phys. Lett.* **1982**, *91*, 348. (b) Katz, B. A.; Strause, C. E. *J. Am. Chem. Soc*. **1979**, *101*, 6214. (c) Romstedt, H.; Hauser, A.; Spiering, H. *J. Phys. Chem. Solids* **1997**, *59*, 265. (d) Romstedt, H.; Spiering, H.; Gütlich, P. *J. Phys. Chem. Solids* **1997**, *59*, 1353. (e) Bousseksou, A.; Nasser, J.; Boukheddaden, K.; Varret, F. *J. Phys*. **1992**, *2*, 1381. (f) Sasaki, N.; Kambara, T. *Phys. Rev. B* **1989**, *40*, 2442. (g) Boinnard, D.; Bousseksou, A.; Dworkin, A.; Savariault, J.-M.; Varret, F.; Tuchagues, J.-P. *Inorg. Chem*. **1994**, *33*, 271. (h) Matouzenko, G. S.; Létard J.-F.; Lecocq, S.; Bousseksou, A.; Capes, L.; Salmon, L.; Perrin, M.; Kahn, O.; Collet, A. *Eur. J. Inorg. Chem*. **2001**, 2935. (i) Dova E.; Stassen A. F.; Driessen, R. A. J.; Sonneveld, E.; Goubitz, K.; Peschar, R.; Haasnoot, J. G.; Reedijk, J.; Schenk, H. *Acta Crystallogr.* **2001**, *B57*, 531. (j) Reedijk, J.; Haasnoot, J. G.; Roubeau, O.; Stassen, A. F. *Mol. Cryst. Liq. Cryst*. **2002**, *379*, 341. (k) Garcia, Y.; Kahn, O.; Rabardel, L.; Chansou B.; Salmon. L.; Tuchagues, J. P. *Inorg. Chem*. **1999**, *38*, 4663.

(15) (a) Mikami, M.; Konno, M.; Saito, Y. *Chem. Phys. Lett.* **1979**, *63*, 566. (b) Mikami, M.; Konno, M.; Saito, Y. *Acta Crystallogr. B* **1980**, *B36*, 275. (c) Mikamikido, M.; Saito, Y. *Acta Crystallogr. B* **1982**, *B38*, 452. (d) Wiehl, L.; Kiel, G.; Köhler, C. P.; Spiering, H.; Gütlich, P. *Inorg. Chem.* **1986**, *25*, 1565. (e) Létard, J.-F.; Guionneau, P.; Rabardel, L.; Howard, J. A. K.; Goeta, A. E.; Chasseau, D.; Kahn, O. *Inorg. Chem*. **1998**, *37*, 4432.

(16) (a) Gütlich, P.; Jung, J. *J. Mol. Struct*. **1995**, *347*, 21. (b) Guionneau, P.; Létard, J.-F.; Yufit, D. S.; Chasseau, D.; Bravic, G.; Goeta, A. E.; Howard, J. A. K.; Kahn, O. *J. Mater. Chem*. **1999**, *9*, 985.

(17) (a) Müller, E. W.; Spiering, H.; Gütlich, P. *Chem. Phys. Lett.* **1982**, *93*, 567. (b) Gallois, B.; Real, J.-A.; Hauw, C.; Zarembowitch, J. *Inorg. Chem.* **1990**, *29*, 1152.

(18) Ménage, S.; Vitrols, S. E.; Bergerat, P.; Codjovi, E.; Kahn, O.; Girerd, J.-J.; Guillot, M.; Solans, X.; Calvert, I. *Inorg. Chem.* **1990**, *30*, 2666.

perturbation is then

$$\mathscr{H}_{\text{trimer}} = -2J(S_1 \cdot S_2 + S_2 \cdot S_3) - 2J_{13}(S_3 \cdot S_1) + \mu_B g(S_1 + S_2 + S_3)H \quad (4)$$

and the Van Vleck expression of magnetic susceptibility for trimer, χ_{trimer}, is

$$\chi_{\text{trimer}} = \frac{Ng^2{\mu_B}^2}{3k_BT} \frac{\sum_S S(S+1)(2S+1)e^{-(E(S_T,S_{13})/k_BT)}}{\sum_S (2S+1)e^{-(E(S_T,S_{13})/k_BT)}} \quad (5)$$

which is a formidable analytical expression that is supplied as Supporting Information. The total spin Hamiltonian, $\mathscr{H}_{\text{tot}}$, taking into further account the molecular-field approximation, is

$$\mathscr{H}_{\text{tot}} = -2J(S_1 \cdot S_2 + S_2 \cdot S_3) - 2J_{13}(S_3 \cdot S_1) + \mu_B g(S_1 + S_2 + S_3)H - 2zJ'\langle S_z \rangle S_z \quad (6)$$

With the molecular-field approximation χ_{trimer} the susceptibility can be expressed as

$$\chi_{\text{tot}} = \frac{\chi_{\text{trimer}}}{1 - \frac{2zJ'}{Ng^2{\mu_B}^2}\chi_{\text{trimer}}} + \text{TIP} \quad (7)$$

where g is the Lande g-value, μ_B is the Bohr Magneton, k_B is the Boltzmann constant, TIP is the temperature independent paramagnetism, and N is Avogadro's number.

The observed data for $[Fe^{III}{}_3O(OAc)_6\mathbf{1}_3][ClO_4]$ as $\mu_{\text{eff}}(T)$ is fit to eq 7 assuming (i) an equilateral arrangement of Fe^{III} ions, i.e., $J = J_{13}$ with the best fit with $J = -29.4$ cm^{-1}, $g = 2.00$, and no TIP; however, although it fits well above 140 K, it is a poor fit below 50 K (Figure 5 inset). By assuming (ii) an isosceles arrangement of Fe^{III} ions, as observed in the structure, i.e., $J \neq J_{13}$ with the best fit with $J = -34.3$ cm^{-1}; $J_{13} = -28.7$ cm^{-1} ($zJ = 0$), $g = 2.00$, and TIP $= 300 \times 10^{-6}$ emu/mol Fe^{III};[20] that fits well above 23 K (Figure 5 inset). These values are in accord with those reported for related iron(III) trimers.[21] To improve the fit, an intermolecular interaction, zJ', as provided by molecular-field approximation (iii), was introduced with $J = -32.5$ cm^{-1}, $J_{13} = -27.1$ cm^{-1}, zJ' of -4.2 cm^{-1}, $g = 2.00$, and TIP $= 300 \times 10^{-6}$ emu/mol Fe^{III}, and gives the best fit down to 2 K (Figure 5 inset) and chi-squared agreement factor $= \sum(\mu_{\text{exp}} - \mu_{\text{calc}})^2/\mu_{\text{exp}}{}^2$ [22] $= 4.43 \times 10^{-3}$ for the data from 2 to 300 K. The value of the zJ' is in good agreement with that reported for the isosceles triangular arrangement of Fe^{III} ions in $(NH_4)[Fe(\mu_3\text{-}OH)(H_2L)_3(HL)_3]$ (H_3L = orotic acid) with $J = -18$ cm^{-1}, $J_{13} = -31.2$ cm^{-1}, and $zJ' = -1.0$ cm^{-1}, although an analytical expression for the susceptibility is not reported,[23] and $J = -27.06$ cm^{-1} and $zJ' = -2.59$ cm^{-1} reported for the equilateral triangular arrangement of Fe^{III} ions in $[Fe_3O(\mu_3\text{-}O_2CPh)_6](NO_3)$.[24] The values of J and J_{13} are typical for the J values reported for related triiron(III) compounds.[25,26]

Conclusion

$[Fe\mathbf{1}_6][ClO_4]_2$ contains two crystallographically unique iron sites, albeit with similar ligand orientation, and a single-step spin transition that occurs at 213 K with hysteresis. The subtle structural differences between the orientational isomers Fe1 and Fe2 of $[Fe\mathbf{1}_6][BF_4]_2$ lead to slight differences in the Fe(II)−N bond distances and consequently Δ_o for each Fe(II) site giving rise to a two-step spin transition. Examination of the magnetic data together with the crystallographic evidence for $[Fe^{II}\mathbf{1}_6][BF_4]_2$, Fe1 and Fe2 can be assigned to the spin transitions at 91 and 192 K, respectively. $[Fe^{II}\mathbf{1}_6][BF_4]_2$ is the first material that exhibits a two-step spin transition with a simultaneous crystallographic phase transition, but does not exhibit thermal hysteresis.

Additionally, a new route to preparing Fe(III) trimers via the oxidation of Fe(II) has also been reported and the new $[Fe_3O(OAc)_6\mathbf{1}_3][ClO_4]$ complex was made with a room-temperature moment of 3.34 μ_B and $J = -32.5$ cm^{-1}, $J_{13} = -27.1$ cm^{-1}, $zJ' = -4.2$ cm^{-1}, and $g = 2.00$.

Acknowledgment. We thank Philipp Gütlich for helpful discussions, and we gratefully acknowledge the support in part from the National Science Foundation Grant CHE 0110685 and U.S. Department of Energy Department of Basic Science Grant DE FG 03-93ER45504.

Note Added after ASAP: The version of this paper posted ASAP on August 5, 2003, contained several errors in Table 1. The table is correct in the version posted on August 12, 2003.

Supporting Information Available: X-ray CIF files for $[Fe\mathbf{1}_6][BF_4]_2$ at 130 and 260 K, $[Fe\mathbf{1}_6][ClO_4]_2$, and $[Fe_3O(OAc)_6\mathbf{1}_3][ClO_4]$ (these have also been deposited with the Cambridge Crystallographic Data Center, ref CCDC-190229, CCDC-190231, and CCDC 190230, respectively); table of eigenvalues for $\mathscr{H}$ from eq 3; and the analytical expression for χ_{trimer}, eq 5. This material is available free of charge via the Internet at http://pubs.acs.org.

IC034226P

(19) Tong, M.-L.; Chen, X.-M.; Sun, Z.-M.; Hendrickson, D. M. *Trans. Met. Chem.* **2001**, *26*, 195. Ernshaw, A.; Figgis, B. N.; Lewis, J. *J. Chem. Soc. A* **1966**, 1656.

(20) The TIP is in accord with values previously reported, e.g., 160, 335, 140×10^{-6} emu/mol Fe^{III}. Xu, Z.; Thompson, L. K.; Matthews, C. J.; Miller, D. O.; Goeta, A. E.; Howard, J. A. K. *Inorg. Chem.* **2001**, *40*, 2446. Grapperhaus, C. A.; Mienert, B.; Bill, E.; Weyhermuller, T.; Wieghardt, K. *Inorg. Chem.* **2000**, *39*, 5306. Dutta, S. K.; Beckmann, U.; Bill, E.; Weyhermuller, T.; Wieghardt, K. *Inorg. Chem.* **2000**, *39*, 3355.

(21) Turta, K. I.; Solonencko, A. O.; Bulgak, I. I.; Jovmir, F. K.; Rosenberg, M.; Stelmaszyk, P.; Filoti, G. *J. Radioanal. Nucl. Chem.* **1995**, *190*, 347. Kakos, G. A.; Winter, G. *Aust. J. Chem.* **1969**, *22*, 97. Gorun, S. M.; Papaeftymiou, G. C.; Frankel, R. B.; Lippard, S. J. *J. Am. Chem. Soc.* **1987**, *109*, 4244.

(22) Taylor, J. R. *An Introduction to Error Analysis*; University Science Books: Mill Valley, CA, 1982; p 223.

(23) Raptopoulou, C. P.; Tangoulis, V.; Psycharis, V. *Inorg. Chem.* **2000**, *39*, 4452.

(24) Degang, F. Guoxiong, W.; Wenxia, T.; Kaibei, Y. *Polyhedron* **1993**, *12*, 2459.

(25) Cannon, R. D.; White, R. P. *Prog. Inorg. Chem.* **1988**, *36*, 195.

(26) Dziobkowski, C. T.; Wrobleski, J. T.; Brown, D. B. *Inorg. Chem.* **1981**, *20*, 671.

(27) Baker, W. A.; Bobonich, H. M. *Inorg. Chem.* **1964**, *3*, 1184. Mikami, M.; Konno, M.; Saito, Y. *Chem. Phys. Lett.* **1979**, *63*, 566.